Asymmetric Mutualism in Two- and Three-Dimensional Range Expansions

Maxim O. Lavrentovich* and David R. Nelson†
Department of Physics, Harvard University, Cambridge, Massachusetts 02138, USA
(Received 24 August 2013; published 1 April 2014)

Genetic drift at the frontiers of two-dimensional range expansions of microorganisms can frustrate local cooperation between different genetic variants, demixing the population into distinct sectors. In a biological context, mutualistic or antagonistic interactions will typically be asymmetric between variants. By taking into account both the asymmetry and the interaction strength, we show that the much weaker demixing in three dimensions allows for a mutualistic phase over a much wider range of asymmetric cooperative benefits, with mutualism prevailing for any positive, symmetric benefit. We also demonstrate that expansions with undulating fronts roughen dramatically at the boundaries of the mutualistic phase, with severe consequences for the population genetics along the transition lines.

DOI: 10.1103/PhysRevLett.112.138102 PACS numbers: 87.15.Zg, 87.10.Hk, 87.18.Tt, 87.23.Cc

When a population colonizes new territory, the abundance of unexploited resources allows the descendants of the first few settlers to thrive. These descendants invade the new territory and form genetically distinct regions or sectors at the population frontier. If the frontier population is small, the birth and death of individuals create large fluctuations in the sector sizes. These fluctuations, called genetic drift, cause some settler lineages to become extinct as neighboring sectors engulf their territory. Over time, this sector coarsening process dramatically decreases genetic diversity at the frontier [1,2].

Interactions between the organisms can modify the coarsening process. For example, cooperative interactions, in which genetic variants in close proximity confer growth benefits upon each other, can lead to the founders' progeny remaining intermingled. Then, coarsening does not occur, and the consequent growth pattern is called a "mutualistic phase" [3]. Cooperative interactions are commonly found in nature: microbial strains exchange resources [4], ants protect aphids in exchange for food [5], and different species of mammals share territory to increase foraging efficiency [6]. Recently, a mutualistic phase was experimentally realized in partner yeast strains that feed each other [7,8]. These experiments require an understanding of *asymmetric* interactions where species do not benefit equally from cooperation. Antagonistic interactions may also occur, e.g., between bacterial strains secreting antibiotics against competing strains [9]. These interactions and the mutualistic phase also play prominent roles in theories of nonequilibrium statistical dynamics [3,10–15].

We explore here asymmetric cooperative and antagonistic interactions in two- and three-dimensional range expansions. Two-dimensional expansions ($d = 1 + 1$) occur when the population grows in a thin layer, such as in a biofilm or on a Petri dish. Three-dimensional expansions ($d = 2 + 1$) occur, for example, at the boundaries of growing avascular tumors [16–18]. We model both flat and rough interfaces at the frontier, the latter being an important feature of many microbial expansions [19].

We arrive at the following biologically relevant results: Three-dimensional range expansions support mutualism more readily than planar ones, and a mutualistic phase occurs for *any* symmetric cooperative benefit. Conversely, two-dimensional expansions require a critical benefit [3,10]. In addition, we find that the frontier roughness is strongly enhanced at the onset of mutualism for asymmetric interactions. Finally, we find that frontier roughness allows for a mutualistic phase over a wider range of cooperative benefits.

Flat front models.—We consider two genetic variants, labeled black and white. Cells divide only at the population frontier [1]. Such expansions occur when nutrients are absorbed before they can diffuse into the interior of the population, inhibiting cell growth behind the population front. This can occur in tumor growth [18] and in microbial expansions at low nutrient concentrations [20].

According to a continuum version of a stepping stone model [3,21], the coarse-grained fraction of black cells $f \equiv f(\mathbf{x}, t)$ at some position $\mathbf{x}$ along a *flat* population front at time t obeys

$$\partial_t f = D\nabla^2 f + \tau_g^{-1} f(1-f)\left[s\left(\frac{1}{2} - f\right) + \frac{r}{2}\right] + \eta, \quad (1)$$

where D is a diffusivity, $\eta(\mathbf{x}, t)$ an Îto noise term [1] with $\langle \eta(\mathbf{x}, t)\eta(\mathbf{x}', t)\rangle = 2\ell^{d_s}\tau_g^{-1} f(1-f)\delta(\mathbf{x}-\mathbf{x}')\delta(t-t')$, τ_g a generation time, d_s the spatial dimension, and ℓ an effective lattice spacing. Also, $r = \alpha - \beta$ and $s = \alpha + \beta$, where α and β represent the increase in growth rates over the base rate per generation of the black and white species, respectively, in the presence of the other species. Equation (1) describes the behavior of two-dimensional expansions of mutualistic strains of yeast [7] and is expected to characterize many different range expansions [1,3]. At $r = s = 0$, Eq. (1) reduces to the Langevin equation of the voter model [14,15]. A signature of the mutualistic phase is a nonzero

average density $\langle\rho\rangle$ of black and white cell neighbors (genetic sector interfaces) at the front at long times. To construct phase diagrams for our different models in Fig. 1, we calculate $\langle\rho\rangle$ as a function of the cooperative benefits α, $\beta \geq 0$ and antagonistic interactions α, $\beta < 0$.

We propose a microscopic model for flat fronts in the spirit of Grassberger's cellular automaton [26], which obeys Eq. (1) under an appropriate coarse graining, as we verify in the following. Domain wall branching, shown in Fig. 2(a), is required for a mutualistic phase in $d = 1 + 1$ dimensions. Our model allows branching by having three cells compete to divide into a new spot on the frontier during each time step. To approximate cell rearrangement at the frontier, we assume that the order of competing cells in each triplet is irrelevant. The update rules are

$$\begin{aligned} p\left(\begin{smallmatrix}\circ\bullet\circ\\ \Downarrow\\ \bullet\end{smallmatrix}\right) &= p\left(\begin{smallmatrix}\bullet\circ\circ\\ \Downarrow\\ \bullet\end{smallmatrix}\right) = p\left(\begin{smallmatrix}\circ\circ\bullet\\ \Downarrow\\ \bullet\end{smallmatrix}\right) = \frac{1}{3} + \alpha \\ p\left(\begin{smallmatrix}\bullet\circ\bullet\\ \Downarrow\\ \circ\end{smallmatrix}\right) &= p\left(\begin{smallmatrix}\circ\bullet\bullet\\ \Downarrow\\ \circ\end{smallmatrix}\right) = p\left(\begin{smallmatrix}\bullet\bullet\circ\\ \Downarrow\\ \circ\end{smallmatrix}\right) = \frac{1}{3} + \beta \\ p\left(\begin{smallmatrix}\bullet\bullet\bullet\\ \Downarrow\\ \bullet\end{smallmatrix}\right) &= p\left(\begin{smallmatrix}\circ\circ\circ\\ \Downarrow\\ \circ\end{smallmatrix}\right) = 1, \end{aligned} \qquad (2)$$

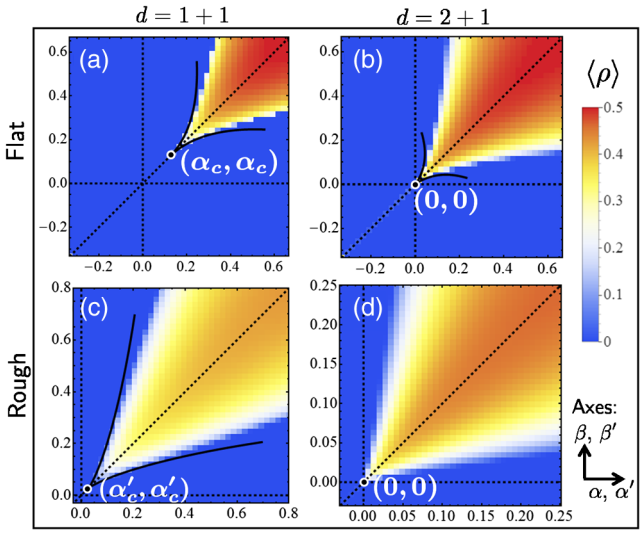

FIG. 1 (color online). The density $\langle\rho\rangle$ of genetic sector interfaces along the population front at long times t (measured in generations), averaged over 10^3 runs of the flat [(a) and (b)] and rough [(c) and (d)] front range expansion models for $d = 1 + 1$ [(a) and (c)] and $d = 2 + 1$ [(b) and (d)] (system sizes L and L^2 cells, respectively) for cooperative benefits α and β defined in Eq. (2) [α' and β' for rough fronts in Eq. (5)]. The parameters are (a) $t = 1.5 \times 10^5$, $L = 8 \times 10^3$; (b) $t = 3 \times 10^3$, $L^2 = 600^2$; (c) $t = 2.5 \times 10^3$, $L = 10^3$; (d) $t = 500$, $L^2 = 50^2$. There is a mutualistic phase in the $\alpha, \beta > 0$, ($\alpha', \beta' > 0$) quadrant in all panels. The solid lines in (a),(b), and (c) show the directed percolation (DP) transition line shapes near the bicritical points (see the Supplemental Material [22]). A symmetric DP (DP2) point occurs at $\alpha = \beta = \alpha_c = 0.1242(5)$ in (a) and a "rough DP2" point at $\alpha' = \beta' = \alpha_c{}' = 0.0277(2)$ in (c). The dotted lines indicate the loci $\alpha = 0$, $\beta = 0$, and $\alpha = \beta$.

where $-1/2 \leq \alpha, \beta \leq 2/3$. The rules for all other combinations follow from probability conservation. Positive α (β) biases the propagation of a black (white) cell into the next generation, due to beneficial goods (e.g., an amino acid in short supply [7]) generated by two nearby cells of the opposite type. Negative α and β represent the effect of cells inhibiting the growth of neighboring competing variants.

For $d = 1 + 1$, the model is implemented on a square lattice (with one space and one time direction) with periodic boundary conditions in the spatial direction. During each generation (one lattice row along the spatial direction), the states of all triplets of adjacent cells are used to determine the state of the middle cell in the next generation using Eq. (2). For $d = 2 + 1$, we stack triangular lattices of cells (representing successive generations) in a hexagonal close-packed three-dimensional array. Each cell sits on top of a pocket provided by three cells in the previous generation, so Eq. (2) generalizes immediately (see the Supplemental Material [22]).

These simple flat front models generate the rich phase diagrams of Figs. 1(a) and 1(b). The $d = 1 + 1$ diagram in Fig. 1(a) resembles the stepping stone model result [3]. One feature is a DP2 point, located at $(\alpha, \beta) = (\alpha_c, \alpha_c) \approx (0.1242, 0.1242)$ in our model. Applying a symmetry-breaking coefficient $r \equiv \alpha - \beta \neq 0$ biases the formation of either black ($r > 0$) or white ($r < 0$) cell domains, and the DP2 transition crosses over to DP transitions along a symmetric pair of critical lines $s_c(r) \equiv \alpha_c(r) + \beta_c(r)$ for

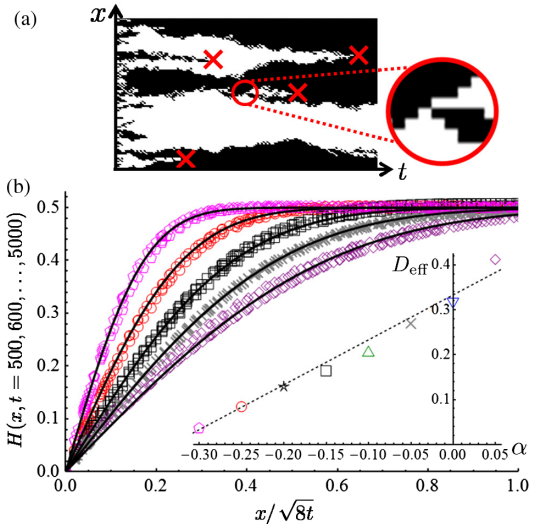

FIG. 2 (color online). (a) A sample evolution of the flat front model for $d = 1 + 1$ at $\alpha = \beta = 0$ (front size $L = 100$). The rules in Eq. (2) allow interface branching (circled event), facilitating mutualistic mixing. The coarse-grained dynamics for $\alpha = \beta < \alpha_c$ are dominated by pair annihilations of interfaces (marked by crosses) [12,13]. (b) We collapse the heterozygosity $H(x, t)$, averaged over 1600 runs with $L = 10^3$, at different times (points in main plot) and fit to Eq. (3) (solid lines) to find D_{eff} in the inset. The dashed line indicates the prediction $D_{\text{eff}} = 1/3 + \alpha$ (see the Supplemental Material [22]).

$r < 0$ and $r > 0$. As in typical cross-over phenomena [27], the phase boundaries near the DP2 point are given by $r \sim \pm[s_c(r) - s_c(0)]^{\phi}$, where $s_c(0) = 2\alpha_c \approx 0.2484$ and ϕ is a cross-over exponent [28]. We find $\phi \approx 1.9(1)$, consistent with studies of related models [22,29]. Hence, we confirm that our model is in the same universality class as Eq. (1). Thus, many features of our nonequilibrium dynamical models near the transition lines (e.g., the power laws governing the phase boundary shape) will also appear in the various range expansions describable by Eq. (1).

We now study the approach to the DP2 point along the $\alpha = \beta$ line for $\alpha < \alpha_c$. As α increases from $-1/3$ to $\alpha_c > 0$, domain boundaries between white and black sectors diffuse more vigorously. To check that the entire line $-1/3 < \alpha < \alpha_c$ with $\alpha = \beta$ is dominated at long wavelengths by the annihilation of domain wall pairs [see Fig. 2(a)], we study the heterozygosity correlation function $H(x,t) = \langle f(x+y,t)[1-f(y,t)] + f(y,t)[1-f(x+y,t)]\rangle$, where $\langle \ldots \rangle$ is an ensemble average and an average over points y along the front [1]. For a random initial condition of black and white cells in equal proportion, $H(x,t)$ can be fit to

$$H(x,t) = \frac{1}{2}\mathrm{erf}\left[\frac{x}{\sqrt{8D_{\mathrm{eff}}t}}\right], \tag{3}$$

where the fitting parameter D_{eff} is the effective diffusivity of the domain walls [1]. The dependence of D_{eff} on α away from the DP2 point is consistent with a simple random walk model of domain walls (see the Supplemental Material [22]), which predicts $D_{\mathrm{eff}} \approx 1/3 + \alpha$ [inset of Fig. 2(b)]. As we approach the DP2 point ($\alpha \to \alpha_c^-$) and domain wall branching becomes important, we observe violations of Eq. (3), consistent with field theoretic studies [12,13].

When $d = 2+1$, two-dimensional domains at the voter model point $\alpha = \beta = 0$ lack a surface tension and readily "dissolve" [15,30]. Our simulations show that these dynamics allow for a mutualistic phase for all $\alpha = \beta > 0$, with a remarkable pinning of the corner of the "wedge" of mutualism in Fig. 1(b) to the origin. A similar phenomenon occurs in branching and annihilating random walks, where an active phase exists for any nonzero branching rate for $d = 2+1$ [13]. However, our model is equivalent to the random walk model only for $d = 1+1$ [14], and the potential connection in higher dimensions is subtle. We now describe how we find the shape of the mutualistic wedge for $d = 2+1$.

When $r = 0$, we find a voter model transition at $s = s_c(r=0) = 0$, and *any* $s > 0$ pushes the system into a mutualistic phase with a nonzero steady-state domain interface density. A perturbation $r \neq 0$ pushes the system away from the voter model class by suppressing interface formation and induces a DP transition at some $s_c(r) > 0$. Upon exploiting cross-over results for a similar perturbation in Ref. [31], we find phase boundaries given by $r \sim \pm s_c(r)/\ln[s_c(r)/s_0]$, where $s_0 \approx 0.551$ is a nonuniversal constant found by fitting. The resulting curves, plotted in Fig. 1(b), agree well with simulations (see the Supplemental Material [22]).

When $\alpha = \beta < 0$ for $d = 2+1$, we find dynamics similar to a kinetic Ising model with a nonconserved order parameter quenched below its critical temperature with an interface density decay $\langle \rho \rangle \sim t^{-1/2}$ [22,30]. A local "poisoning" effect penalizes domain wall deformations, creating an effective line tension σ between domains. To find σ, we evolve initially flat interfaces of length L to an approximate steady state. Fluctuations in the interface position $h(x)$ are characterized by its Fourier transform $h(q)$. Upon averaging over many realizations, we expect that, in analogy with capillary wave theory [27],

$$\langle |h(q)|^2 \rangle = \frac{k_B T}{\sigma L q^2}, \tag{4}$$

where T is an effective temperature. Figure 3 shows that the dimensionless line tension σ/k_BT increases as α becomes more negative and that Eq. (4) gives the correct prediction for $\langle |h(q)|^2 \rangle$. As we approach the voter model point ($\alpha \to 0^-$), σ/k_BT vanishes with an apparent power law $\sigma/k_BT \sim |\alpha|^{0.61}$. However, models with stronger noise might have a voter-model-like coarsening for $\alpha = \beta < 0$, instead [32].

Rough front models.—We model range expansions with rough frontiers using a modified Eden model which tracks cells with at least one empty nearest or next-nearest neighbor lattice site [33]. Each such "active" cell i has a birth rate

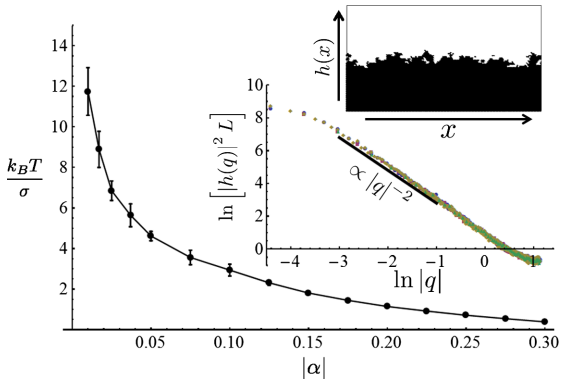

FIG. 3 (color online). The main plot shows the effective, dimensionless inverse line tension k_BT/σ in $d = 2+1$ dimensions [see Eq. (4)] for negative α (line guides the eye). Results are from the final interface position $h(x)$ in simulations of an initially flat interface of length $L = 512$ evolved for $t \gtrsim 7000$ generations. The interface has overhangs and holes, and $h(x)$ is the average position for each x. The upper right inset is a sample interface for $L = 128$ and $t = 500$. In the remaining inset, we confirm that Eq. (4) correctly predicts the scaling with L by collapsing the Fourier-transformed height $h(q)$, averaged over 160 runs, for $L = 128, 256, 512, 1024$.

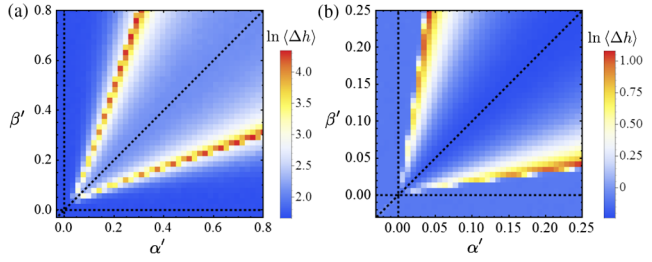

FIG. 4 (color online). The fluctuation $\langle\Delta h(t)\rangle$ of the rough frontier (averaged over 10^3 runs) of a range expansion with (a) $d = 1 + 1$ with $L = 10^3$ cells at time $t = 2.5 \times 10^3$ generations and (b) $d = 2 + 1$ with $L = 50^2$ cells at time $t = 500$ generations. The black dotted lines indicate the loci $\alpha' = 0$, $\beta' = 0$, and $\alpha' = \beta'$.

$$b_i = \frac{1}{3} + \alpha' N_w(i) \quad \text{or} \quad b_i = \frac{1}{3} + \beta' N_b(i), \tag{5}$$

if the cell is black or white, respectively. We set the background birth rates (i.e., for populations of all-black or all-white cells) to $1/3$ to make contact with a neutral flat front model. $N_{b,w}(i)$ denote the number of black and white nearest neighbors of cell i, respectively.

At each time step, we pick an active cell i to divide into an adjacent, empty lattice site with probability b_i/b_{tot}, where b_{tot} is the sum of the active cell birth rates. For $d = 1 + 1$, cells can divide into next-nearest neighbor spots to allow for domain boundary branching (see the Supplemental Material [22]). When computing quantities such as the interface density, we wait for the undulating front to pass and then take straight *cuts* through the population parallel to the initial inoculation. The distance of the cuts from the initial inoculation defines our time coordinate.

At the voter model point $\alpha' = \beta' = 0$, the roughness of the front is insensitive to the evolutionary dynamics and genetic domain walls inherit the front fluctuations [19,34]. The average interface density satisfies $\langle\rho(t)\rangle \sim t^{-2/3} \sim t^{-1/\tilde{z}}$ [34], where $\tilde{z} = 3/2$ represents the dynamical critical exponent associated with the Kardar-Parisi-Zhang equation [35], or equivalently, the noisy Burgers equation [36]. We find that the interface density obeys this scaling for *all* $\alpha' = \beta' < \alpha_c'$ (see the Supplemental Material [22]). Rough fronts yield novel critical behavior at the DP2 point for $d = 1 + 1$: The cross-over exponent governing the shape of the phase diagram in Fig. 1(c) decreases considerably to $\phi' \approx 1.27(15)$, from $\phi \approx 1.9(1)$ for flat fronts. This change leads to a wider mutualistic wedge near the DP2 point. In addition, we find a power law decay of the interface density, $\langle\rho(t)\rangle \sim t^{-\theta'_{\text{DP2}}}$, with a dramatically different critical exponent $\theta'_{\text{DP2}} \approx 0.61(1)$ compared to $\theta_{\text{DP2}} \approx 0.285(5)$ for flat fronts [22,37]. For $d = 2 + 1$, we did not have enough statistics to precisely determine the phase diagram shape. However, the DP2 point again appears to move to the origin.

The front roughness is a remarkable barometer of the onset of mutualism. We characterize the roughness by calculating the interface height $h(\mathbf{x}, t)$ and its root mean square fluctuation $\langle\Delta h(t)\rangle \equiv \sqrt{\langle(h(\mathbf{x}, t) - \langle h(\mathbf{x}, t)\rangle)^2\rangle}$, where $\langle\ldots\rangle$ is both an ensemble average and an average over all points $\mathbf{x}$ at the front. Front fluctuations are greatly enhanced along the pair of DP transition lines for $d = 2 + 1$ and $d = 1 + 1$, as shown in Fig. 4. At long times, the roughness saturates due to the finite system size (see [22,33]).

Conclusions.—To summarize, we found that a mutualistic phase is more accessible in three-dimensional than in two-dimensional range expansions. Also, antagonistic interactions between genetic variants in three dimensions create an effective line tension between genetic domains. The line tension vanishes at a neutral point where the variants do not interact and where the mutualistic phase wedge gets pinned to the origin. In addition to the power laws governing the phase diagram shapes in Figs. 1(a),1(b), and 1(c), we found a striking interface roughness enhancement at the onset of mutualism. These results should apply to a wide variety of expansions because they are insensitive to the microscopic details of our models along transition lines, where we expect universal behavior at large length scales and long times. The existence of universality has been established for flat fronts [11] and a recent study points to a rough DP universality class [33].

It would be interesting to compare two- and three-dimensional range expansions of microorganisms [7,8] to test the predicted pinning of the mutualistic phase to the $\alpha = \beta = 0$ point. In two dimensions, these expansions are readily realized in Petri dishes [38,39]. In three dimensions, one may, for example, grow yeast cell *pillars* on a patterned Petri dish with an influx of nutrients at one end of the column, or study the frontier of a growing spherical cluster in soft agar [40].

We thank M. J. I. Müller and K. S. Korolev for helpful discussions. This work was supported in part by the National Science Foundation (NSF) through Grants No. DMR-1005289 and No. DMR-1306367, and by the Harvard Materials Research Science and Engineering Center via Grant No. DMR-0820484. Portions of this research were done during a stay at the Kavli Institute for Theoretical Physics at Santa Barbara, supported by the NSF through Grant No. PHY11-25915. Computational resources were provided by the Center for Nanoscale Systems (CNS), a member of the National Nanotechnology Infrastructure Network (NSF Grant No. ECS-0335765). CNS is part of Harvard University.

*lavrentm@gmail.com
†nelson@physics.harvard.edu

[1] K. S. Korolev, M. Avlund, O. Hallatschek, and D. R. Nelson, Rev. Mod. Phys. **82**, 1691 (2010).
[2] M. O. Lavrentovich, K. S. Korolev, and D. R. Nelson, Phys. Rev. E **87**, 012103 (2013).

[3] K. S. Korolev and D. R. Nelson, Phys. Rev. Lett. **107**, 088103 (2011).
[4] E. H. Wintermute and P. A. Silver, Mol. Syst. Biol. **6**, 407 (2010).
[5] J. D. Styrsky and M. D. Eubanks, Proc. R. Soc. B **274**, 151 (2007).
[6] C. R. Dickman, Trends Ecol. Evol. **7**, 194 (1992).
[7] M. J. I. Müller, B. I. Neugeboren, D. R. Nelson, and A. W. Murray, Proc. Natl. Acad. Sci. U.S.A. **111**, 1037 (2014).
[8] B. Momeni, K. A. Brileya, M. W. Fields, and W. Shou, eLife **2**, e00230 (2013).
[9] R. A. Long and F. Azam, Appl. Environ. Microbiol. **67**, 4975 (2001).
[10] L. Dall'Asta, F. Caccioli, and D. Beghé, Europhys. Lett. **101**, 18003 (2013).
[11] H. Hinrichsen, Adv. Phys. **49**, 815 (2000).
[12] L. Canet, H. Chaté, B. Delamotte, I. Dornic, and M. A. Muñoz, Phys. Rev. Lett. **95**, 100601 (2005).
[13] J. L. Cardy and U. C. Täuber, J. Stat. Phys. **90**, 1 (1998).
[14] O. Al Hammal, H. Chaté, I. Dornic, and M. A. Muñoz, Phys. Rev. Lett. **94**, 230601 (2005).
[15] I. Dornic, H. Chaté, J. Chave, and H. Hinrichsen, Phys. Rev. Lett. **87**, 045701 (2001).
[16] T. Roose, S. J. Chapman, and P. K. Maini, SIAM Rev. **49**, 179 (2007).
[17] S. Torquato, Phys. Biol. **8**, 015017 (2011).
[18] A. Brú, S. Albertos, J. L. Subiza, J. L. Garcia-Asenjo, and I. Brú, Biophys. J. **85**, 2948 (2003).
[19] O. Hallatschek, P. Hersen, S. Ramanathan, and D. R. Nelson, Proc. Natl. Acad. Sci. U.S.A. **104**, 19926 (2007).
[20] M. O. Lavrentovich, J. H. Koschwanez, and D. R. Nelson, Phys. Rev. E **87**, 062703 (2013).
[21] M. Kimura and G. H. Weiss, Genetics **49**, 561 (1964).
[22] See Supplemental Material at http://link.aps.org/supplemental/10.1103/PhysRevLett.112.138102, which includes Refs. [23–25], for more detailed discussion and additional figures.
[23] A. Gelimson, J. Cremer, and E. Frey, Phys. Rev. E **87**, 042711 (2013).
[24] L. Shapiro and G. Stockman, *Computer Vision* (Prentice Hall PTR, Upper Saddle River, NJ, 2001).
[25] M. E. Fisher and M. N. Barber, Phys. Rev. Lett. **28**, 1516 (1972).
[26] P. Grassberger, F. Krause, and T. von der Twer, J. Phys. A **17**, L105 (1984).
[27] M. Plischke and B. Bergersen, *Equilibrium Statistical Physics* (World Scientific, New Jersey, 2006), 3rd ed.
[28] M. E. Fisher and D. R. Nelson, Phys. Rev. Lett. **32**, 1350 (1974).
[29] G. Ódor and N. Menyhárd, Phys. Rev. E **78**, 041112 (2008).
[30] P. L. Krapivsky, S. Redner, and E. Ben-Naim, *A Kinetic View of Statistical Physics* (Cambridge University Press, Cambridge, England, 2010).
[31] H. K. Janssen, J. Phys. Condens. Matter **17**, S1973 (2005).
[32] D. I. Russell and R. A. Blythe, Phys. Rev. Lett. **106**, 165702 (2011).
[33] J.-T. Kuhr, M. Leisner, and E. Frey, New J. Phys. **13**, 113013 (2011).
[34] Y. Saito and H. Muller-Krumbhaar, Phys. Rev. Lett. **74**, 4325 (1995).
[35] M. Kardar, G. Parisi, and Y.-C. Zhang, Phys. Rev. Lett. **56**, 889 (1986).
[36] D. Forster, D. R. Nelson, and M. J. Stephen, Phys. Rev. A **16**, 732 (1977).
[37] M. Henkel, H. Hinrichsen, and S. Lübeck, *Non-Equilibrium Phase Transitions*, Absorbing Phase Transitions, Vol. I (Springer Science, Netherlands, 2008).
[38] K. S. Korolev, J. B. Xavier, D. R. Nelson, and K. R. Foster, Am. Nat. **178**, 538 (2011).
[39] K. S. Korolev, M. J. I. Müller, N. Karohan, A. W. Murray, O. Hallatschek, and D. R. Nelson, Phys. Biol. **9**, 026008 (2012).
[40] P. Hersen, C. Vulin, and M. J. I. Müller (private communication).